RESEARCH ARTICLE OPEN ACCESS

Fatigue Resistance of Brake System Components Made of Aluminium Alloy

Sergio Baragetti[a,1,2*], Andrea Gavazzi[b,3], Paolo Masiello[c]
[1]Department of Engineering, University of Bergamo, Viale Marconi 5, 24044, Dalmine (BG), Italy
[2] GITT – Centre on Innovation Management and Technology Transfer of the University of Bergamo, Via Salvecchio 19, 24129 Bergamo, Italy.
[3]Adv. R&D – Brembo S.p.A.

Abstract
In this paper the influence of the microstructure, in terms of the DAS index, and of the geometrical notches on the fatigue resistance of a brake system component, made of aluminium alloy, was investigated. G-AlSi7Mg die casting automotive brake calipers were considered in this study and different die casting processes for their production were analyzed. Several experimental fatigue tests on rotating bending specimens were carried out in order to directly correlate the fatigue behaviour and the material microstructure. The effect of the geometry was analyzed by means of pulsating pressure tests on the full scale components, with and without considering the braking torque. Accurate three dimensional FE models of the half brake caliper subject to the highest levels of load were also developed. Different theoretical models, such as the Heywood equation and the Sines criterion, were applied to predict the fatigue life of both the specimens and the component.
Keywords: Brake calipers, aluminium alloy, fatigue, microstructure, FEM.

I. Introduction

Cast light alloys are, for the time being, more and more widely used in the automotive field to reduce the weight of components such as the chassis, the engine block and the braking system (Silva et Al., 2004; Burger et Al, 2005; Carrera et Al., 2007). Therefore, the need for precise knowledge of the influence of constructive parameters becomes a critical issue. In this work the influence of the geometry, loading spectrum and microstructure on the fatigue behaviour of a brake system component made of UNI 3599 - G-AlSi7Mg aluminium alloy were analysed. As far as the authors know, no noteworthy studies about fatigue phenomena on these components are available. The experimental data in the scientific literature also point out a high scatter in the fatigue resistance of casting aluminium components (Xi et Al., 2000; Underhill et Al, 2008; DuQuesnay et Al., 2010). Several studies on the influence of the microstructure on the casting aluminium mechanical properties were also carried out. Initially the research was centred on the evaluation of the Dendrite Arm Spacing (DAS) index and on the correlation between that parameter and the static and fatigue resistance (Linder et Al., 2006; Min et Al., 2009). Afterwards, further studies highlighted that the DAS parameter is important for estimation of the static, but not for the fatigue resistance. As a matter of fact, the thermal treatments could modify the material microstructure in terms of micro and macro defects and impurities. Models based on the fracture mechanics were developed in order to estimate the influence of the defect dimension on the fatigue behaviour, taking into account the effect of both the microstructure and the stress concentration factor due to the particular geometry of the component. Initially, the mechanical properties and the density of the alloy were experimentally evaluated by obtaining three series of specimens from different castings. Standard (degassed and cooled), non-degassed and non-cooled casting processes were considered. The DAS parameter was also evaluated for each type of casting. Fatigue tests were carried out both on standard hourglass specimens, following the staircase method, and on full-scale components in order to point out the effect of the material microstructure and the notch size on the fatigue behaviour. Several FE models of the brake caliper were also developed with the aim of evaluating the stress-strain state and estimating the stress concentration factor in the most critical areas. The numerical models were confirmed by the experimental tests and the results highlighted that, although a fine microstructure has a beneficial influence on the static resistance, the fatigue behaviour is influenced more strongly by the presence of geometrical notches (Tokaji, 2005). The geometry of the components proved to be the main aspect influencing the fatigue behaviour. However, the geometry of a component, such as a brake caliper object of this study, is often critical and difficult to modify. An accurate control of the material microstructure could, then, be reasonably considered to improve the fatigue resistance.

II. Material properties

In accordance with the UNI-EN-1706 and UNI-EN-1676 European Standards, the aluminium alloy G-AlSi7Mg was used to obtain a series of brake calipers by means of the gravity die casting process. Two different castings were considered: the former, called standard and the latter called non-degassed, from which the standard and non-degassed brake calipers were melded respectively. The brake calipers named chill-off were also obtained by means of a non-cooled die casting from standard casting. The chemical compositions of the different castings (Masiello, 1998) are reported in Table 1.

The effective gas quantity dissolved on the liquid metal was evaluated by measuring the metal density with the gravimetric method during the different phases of the production cycle. The results of the density measures for each type of casting during the die casting process are shown in Fig. 1.

Tensile tests and microscopic observations on the metallographic sections were also carried out on samples taken during the casting process. The microstructure was evaluated by measuring the dendrite arm spacing (DAS) defined as the distance between the contiguous dendrite arms and measured in μm. The dimension of the dendrites is influenced by the alloy chemical composition and the casting phase. In particular, the most important parameter is the heat transfer rate during solidification. In fact, the smaller the DAS value results are, the smaller the defect dimension formed during the eutectic solidification is. The tensile test results and the quality index (DAS) obtained are reported in Table 2, while the micrographs of the sample sections are shown in Fig. 2. The results pointed out the connection between the static mechanical properties and the DAS index.

The castings were finally subject to solution heat-treatment at 540°C for 10 hours, followed by water quenching and ageing treatments at 185°C for 8 hours.

The literature data (Suresh, 1991) show that, in the Coffin-Manson's diagram of a typical AlSi7Mg alloy cyclic behaviour, the elastic deformation prevails for 350,000 fatigue cycles.

III. Experimental tests

In order to correlate the microstructure and fatigue life without considering the influence of the geometry, fatigue tests on the smooth specimens were carried out. According to the typical fatigue life of the braking system components, a maximum number of cycles of 350,000 was selected. To assess the influence of the stress concentration factor due to the complex geometry of the brake caliper, experimental fatigue tests were also carried out on the full scale components. The brake calipers were tested by applying different levels of a pulsating braking pressure and also by considering the presence of the constant braking torque. The rotating bending tests on the specimens and the fatigue tests on the brake calipers are described in the following sections.

3.1. Rotating bending tests

Rotating bending tests (R = -1) were carried out on standard hourglass-shaped specimens with the geometry shown in Fig. 3(a) according to UNI 3964 and ISO 1143 standards. The specimens were machined directly from the brake calipers. In order to verify the absence of parasite bending loads during the tests, two strain gages were bonded along the specimen symmetry plane at the opposite sides. Four strain measures during each rotation were taken for ten rotations, on the whole without evidencing any parasite bending. Fatigue samples were loaded in the 120-160 MPa range; the pitch chosen for the load variation was 10 MPa and the upper limit of the fatigue life was set at 350,000 cycles. In compliance with the standards, the rotation speed was 2300 rpm. Only nine specimens were available: the fatigue limit was calculated by means of the statistical analysis described in the reduced staircase method (Dixon et Al, 1983), which gives an average value of the fatigue limit with a reliability of 50%. The results of the rotating bending tests were collected in the Wöhler diagram shown in Fig. 3(b). The stress level vs. cycles to failure diagram points out a small reduction in the fatigue limit (less than 10%) between the standard and non-degassed or chill-off castings, for a number of cycle equal to 350,000 which represents the typical usage of the brake calipers object of this work. The slope of the interpolation line is approximately the same for the standard and the chill-off specimens, while it is greater for the non-degassed ones. The data collected suggested, furthermore, that the decrease in the fatigue resistance at $2x10^6$ or 10^7 cycles should be higher, especially for the non-degassed castings, as reported in several literature references (González et Al, 2011), where a pronounced effect of the DAS parameter on the fatigue resistance of casting aluminium components is pointed out. The Heywood model (Heywood, 1962; Weibull, 1961) was also used in order to predict the endurance limit with the following equation:

$$\frac{\sigma_a}{UTS} = \frac{1 + 0.0038 \cdot n}{1 + 0.008 \cdot n^4} \quad (1)$$

In equation (1) σ_a is the applied stress amplitude and $n = Log\ (N_f)$ where N_f is the number of cycles to failure for that applied stress. Although the Heywood model was developed for the unlimited fatigue resistance of aluminium alloys, the data extracted with this model for 350,000 fatigue cycles pointed out a good correspondence with the experimental results of fatigue tests for standard and chill-off specimens, as shown in Fig. 4.

3.2. Fatigue tests on brake calipers

As stated previously, fatigue tests on the full scale components were also carried out. The

geometrical notches, due to the complex geometry of the brake calipers, and the machining operations are, in fact, expected to have a considerable effect on the fatigue resistance. In order to obtain grade T6, after the casting process, solution heat-treatment followed by quenching and artificial aging were applied to the brake calipers. After the heat treatments, the contact surfaces, oil cylinder and exterior of the calipers were milled and, after this, the oil circulation conduits and the threaded holes were machined. The brake calipers were then subjected to the hot-trimming process and surface oxidation in order to improve the corrosion and wear resistance.

Two different types of fatigue tests were performed on the brake calipers: coupled constant torque and pulsating pressure tests, which are the most representative of the working conditions of the brake system, and pulsating pressure tests, by means of which different working pressures were tested. The brake calipers were mounted on a beam frame fixed to the ground and the oil pressure in the brake circuit was regulated by means of a hydraulic oil cylinder. The schematic drawing of the tests setup is shown in Fig. 5.

A constant braking torque of approximately 2400 Nm and a pulsating pressure equal to 10 MPa maximum were applied during the pressure/torque tests. The tests were carried out both at ambient temperature and at 200°C, the frequency used was in the 900-1000 cycles/hour range and the upper limit of fatigue life was set at 350,000 cycles.

As regards the second type of tests, different pulsating pressure levels were tested and different upper limits of fatigue life were considered in order to reproduce a typical working load spectrum. The characteristic parameters of the different tests are summarized in Table 3.

The failure of the brake calipers was identified by continuously monitoring the oil pressure in the hydraulic circuit. In fact, the presence of a fatigue crack on the base of the oil cylinder, which is the most critical region, allows the oil to be drawn out, generating a sudden reduction in the pressure in the hydraulic circuit. The results of the fatigue tests on the brake calipers are shown in Fig. 6. All the experimental points are collected in a semi-logarithmic diagram, while the failures which occurred at 14 MPa are plotted in a linear diagram.

The pressure vs. cycles to failure diagram points out a small influence of the microstructure on the fatigue behaviour. The reduction in the fatigue limit for the non-degassed callipers is, in fact, about 10%. The mean value of the number of cycles and the standard errors calculated for the different types of calipers tested at 14 MPa, and the same parameters for the brake calipers tested at 10 MPa with and without the braking torque are reported in Table 4 (a, b).

A direct measure of the strain values, by means of strain gages, in the critical region appeared very difficult to implement because of the inaccessibility of the oil cylinder base. Therefore, in order to compare the results of the experimental tests with suitable FE models (section 4), the displacements of several points of the external surface of the brake calipers were measured using LVDT sensors at different oil pressure levels (from 0.5 to 10 MPa).

The maps of the measured points on the two half-calipers are shown in Fig. 7(a, b), while the results of the displacement measures are collected in Fig. 7(c, d).

IV. Numerical models

A numerical model of the brake caliper subject to the test conditions previously reported was developed and confirmed by the experimental results. The FEM model allows the brake components to be designed with greater accuracy in comparison with the classic machine design models, and their stress-strain state to be better understood. During the pulsating pressure tests, the experimental failures occurred mainly at the half brake caliper fixed to the chassis: thus only this part of the entire brake system was modelled. By considering the symmetry of the geometry, the loads and the boundary conditions, only a half of the complete geometry was simulated. Static linear elastic analyses using the FE Nastran® code were then performed.

The complexity of the model, rich in fillets with small radii and holes for the oil circulation, and the need for homogenous distribution of the elements, required the use of ten-node tetrahedral elements. A suitable mesh refinement was considered at the bottom of the oil cylinder, where the expected stress values could reach high values, as shown in Fig. 8(a). The mesh seed was also increased in the regions with a high stress concentration factor, such as the oil circulation holes and the fillet areas. For the whole model, the number of degrees of freedom processed was about 35,000. Besides considering the symmetry boundary conditions, the connection holes and the contact surface between the two half calipers were fixed to the ground in order to simulate the bolted joint. A uniform pressure was then applied at the bottom of the oil cylinder. The configuration of the loads and boundary conditions is shown in Fig. 8(b).

The results of the numerical simulations showed, as expected, that the most critical area, from the point of view of the maximum principal stress, is located at the bottom of the oil cylinder in correspondence with the oil feeding line. Fig. 9 shows the map of the maximum principal stress in the whole model and the map of the maximum principal stress at the fillet at the bottom of the oil cylinder respectively. In order to confirm the accuracy of the numerical results, the displacements under the action of the 10 MPa pressure were also evaluated. A small difference, of less than 3%, between the numerical displacements and the experimental measures taken

with LVDT sensors was obtained and highlighted the good reliability of the FE models.

V. Fatigue life prediction

The collection of results, in terms of stress-strain state, obtained with the numerical models allows the use of the Sines criterion to calculate a safety factor. In the application of this criterion, the alternating and the mean stress components are separated and, according to the Ros and Heichinger proposal, the octahedral shear stress was selected as the limit stress. With the hypothesis of constant direction of the principal stresses, the alternating octahedral shear stress is given by:

$$\sigma^* = \tau_{oct,alt} = \sqrt{\sigma_{I,alt}^2 + \sigma_{II,alt}^2 + \sigma_{III,alt}^2 - \sigma_{I,alt}\sigma_{II,alt} - \sigma_{II,alt}\sigma_{III,alt} - \sigma_{I,alt}\sigma_{III,alt}} \quad (2)$$

The effect of the mean stress is taken into account by introducing the first invariant of the mean components:

$$\sigma^* \le \left(\frac{\sigma_{FAa}}{\eta}\right) \cdot b_3 - k\left(\sigma_{I,m} + \sigma_{II,m} + \sigma_{III,m}\right) \quad (3)$$

The value of the *k*-factor was calculated by applying the criterion to a well-known load case, such as the axial pulsating one (R = 0). In this case the limit stress is given by:

$$\sigma^* \le \sigma_{FAa} - k\left(\sigma_{alt}^*\right) \quad (4)$$

Where σ^*_{alt} is the alternating axial fatigue limit calculated with the Haigh diagram.

By considering the simplified representation of the Haigh diagram, the *k*-factor represents the slope of the limit line. Assuming a fatigue life equal to 350,000 and 580,000 cycles, the *k*-factor values calculated were 0.48 and 0.45 respectively. For the fatigue life prediction of the brake calipers, the maximum stress components in the most critical area were considered. Therefore, the effect of the geometrical stress concentration factor is taken into account. It is well known that, in case of fatigue loading, the static stress concentration factor (K_t) should be replaced, for each principal component of the stress tensor, by the fatigue stress concentration factor (K_f), which is related to the static stress concentration factor and to the notch sensitivity (q). Due to the complex geometry of the mechanical component considered, nevertheless, a rearrangement of the stress status to take into account the notch sensitivity was not possible. By considering that the fatigue stress concentration factor, which is affected by the notch sensitivity, is always lower than the static one, the principal stresses obtained with the FE analysis could conservatively be used for the fatigue life prediction. The fatigue life prediction data are compared with the experimental results for both the specimens and the brake calipers in Fig. 10. The prediction curves shown were obtained by means of the Sines criterion, with and without considering the effect of the mean stress and they are, respectively, named as complete and alternating Sines model. The diagram indicates that the prediction made using the Sines criterion with the mean stress contribution is far from the experimental curve, while the prediction made considering the Sines criterion without mean stress components has good correspondence with the experimental results. The failure mechanism therefore seems to be dependent mainly on the alternating component of stress. This consideration is further confirmed by observing that the slope of the alternating Sines prediction curve is close to the ones obtained from the alternating fatigue tests, with a zero mean stress component (R = -1), performed on standard specimens and brake calipers.

VI. Conclusions

The aim of this paper was to investigate the effect of geometry and microstructure on the fatigue resistance of aluminium brake calipers by means of experimental tests and numerical models. Different microstructures were taken into account by producing different types of specimens and components. Several fatigue tests were performed both on rotating bending specimens and brake calipers. The results of the former showed a reduction of less than 10% in the fatigue limit between the standard and the other casting types. The material microstructure therefore has a limited influence on the fatigue resistance. The theoretical Heywood model was applied to correlate the experimental results, showing good agreement for the standard and the non-cooled specimens. Pulsating pressure tests with and without considering the braking torque were performed on the brake calipers. Three different levels of braking pressure were applied and different fatigue lives were considered: the test results showed a slight influence of the microstructure on the fatigue behaviour. The FE models developed were confirmed by the experimental results, highlighting that the bottom of the oil cylinder represents the most critical area of the brake calliper, where the stress concentration factor is at its maximum. The collection of numerical results allowed use of the Sines theoretical criterion to predict the fatigue life of the brake calipers. Comparing the predicted and the experimental curves, the failure mechanism turned out to be mainly dependent on the alternating component of stress.

References

[1] Burger, G. B., Gupta, A. K., JeiIrey, W., Lloyd, D. J. (2005). Microstructural Control of Aluminum Sheet Used in Automotive Applications. *Mater. Charact.* 35:23-39.

[2] Carrera, E., Rodrıguez, A., Talamantes, J., Valtierra, S., Colas, R. (2007). Measurement of residual stresses in cast aluminium engine blocks. *J. Mater. Process. Tech.* 189:206–210.

[3] Dixon, W. J., Massey, F. J. (1983). *Introduction to statistical analysis*. New York: McGraw-Hill.
[4] DuQuesnay, D. L., Underhill, P. R. (2010). Fatigue life scatter in 7xxx series aluminum alloys. *Int. J. Fatigue* 32(2):398-402.
[5] González, R., Martínez D. I., Talamantes, J., Valtierra, S., Colás, R. (2011), Fatigue testing of an aluminium cast alloy. *Int. J. Fatigue*, 33:273-278.
[6] Heywood, R. B. (1962). *Designing against fatigue*. London: Clapman and Hall.
[7] Linder, J., Axelsson, M., Nilsson, H. (2006). The influence of porosity on the fatigue life for sand and permanent mould cast aluminium. *Int. J. Fatigue* 28:1752–1758.
[8] Masiello, P. (1998). Influenza della geometria e della microstruttura sulla resistenza a fatica di componenti in G-AlSi7Mg. *Degree thesis, supervisor Prof. Angelo Terranova.* Milano: Politecnico di Milano.
[9] Min, Q., Lin, L., Feng-tao, T., Jun, Z., Heng-zhi, F. (2009). Effect of sample diameter on primary dendrite spacing of directionally solidified Al-4%Cu alloy. *T. Nonferr. Metal. Soc.* 19(1):1-8.
[10] Silva, M. B., Baptista, R. M. S. O., Martins, P. A. F. (2004). Stamping of automotive components: a numerical and experimental investigation. *J. Mater. Process. Tech.* 155–156:1489–1496.
[11] Suresh, S. (1991). *Fatigue of Materials*. Cambridge: Cambridge University Press.
[12] Tokaji, K. (2005). Notch fatigue behaviour in a Sb-modified permanent-mold cast A356-T6 aluminium alloy. *Mater. Sci. Eng.* A396:333–340.
[13] Xi, N. S., Xie, M. L., Zhang, Z. L., Tao, C. H. (2000). Fatigue life scatter of aluminium alloy helicopter lugs. *Eng. Fail. Anal.* 7:239-247.
[14] Underhill, P. R., DuQuesnay, D. L. (2008). The effect of dynamic loading on the fatigue scatter factor for Al 7050. *Int. J. Fatigue* 30(4):614-622.
[15] Weibull, W. (1961). *Fatigue testing and analysis of results*. Oxford: Pergamon Press

Figures

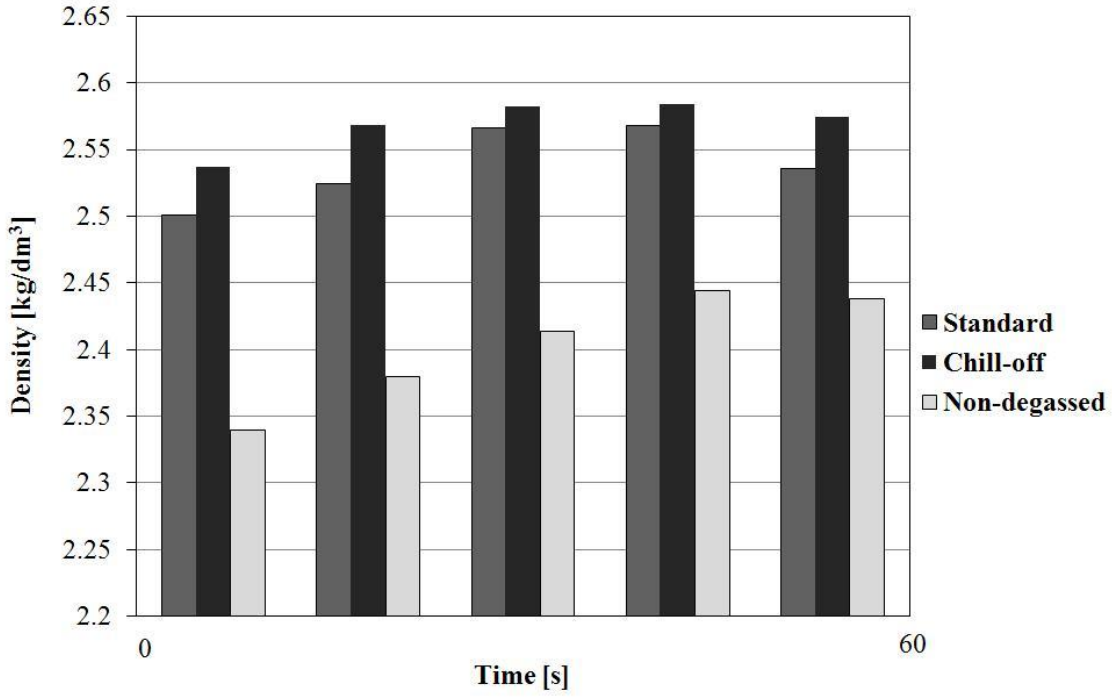

Fig. 1. Diagram of the density measured during the die casting process.

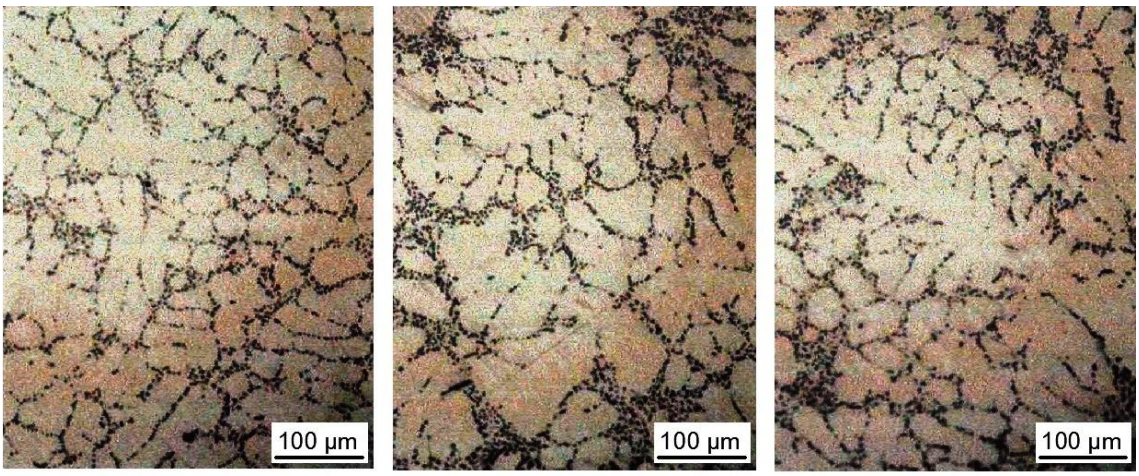

a) **b)** **c)**

Fig. 2. Micrographs (200x) of the sample sections: (a) standard, (b) chill-off and (c) non-degassed castings.

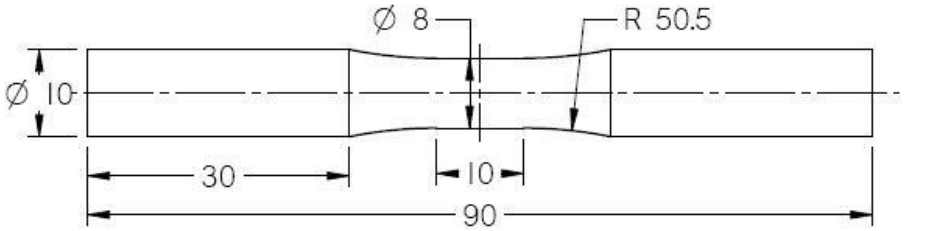

a)

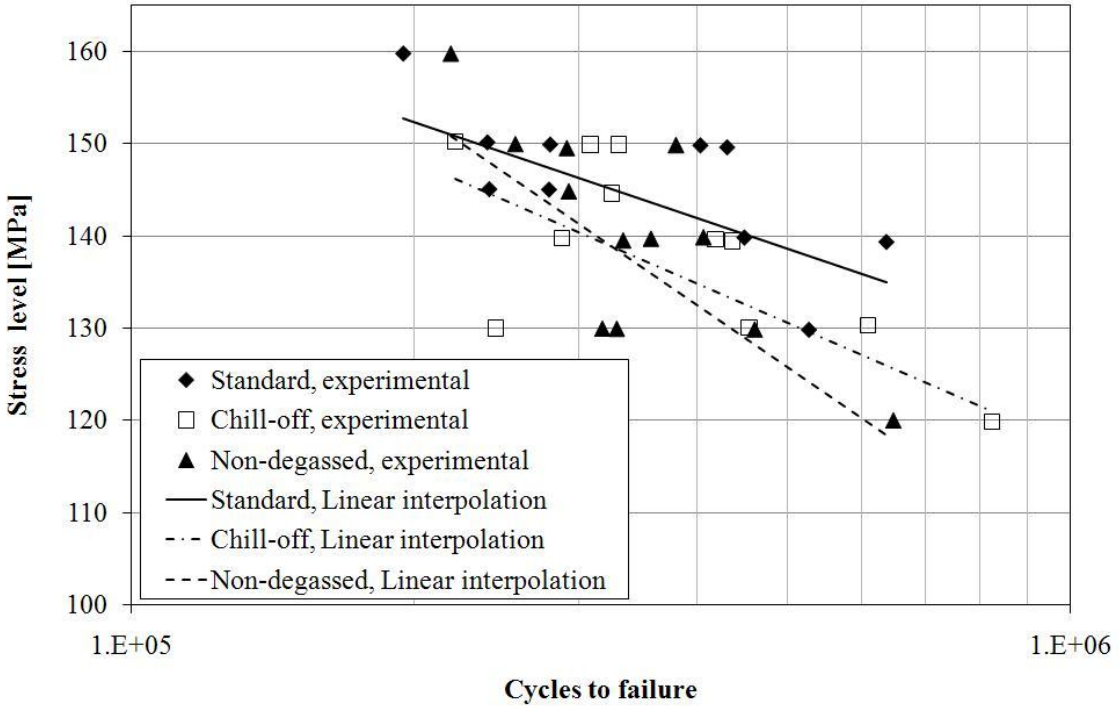

b)

Fig. 3. (a) rotating bending specimen geometry, (b) Wöhler diagram with indication of the experimental points obtained and the linear interpolation for each specimen type.

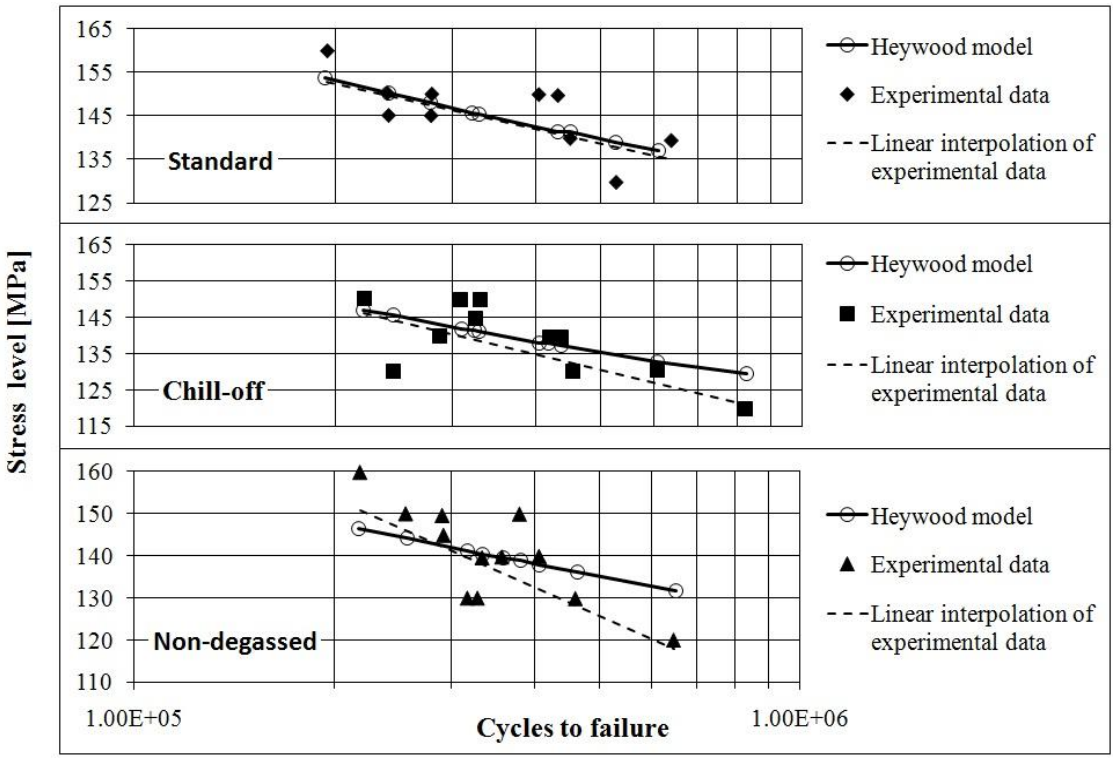

Fig. 4. Comparison between the experimental failures and the Heywood model results.

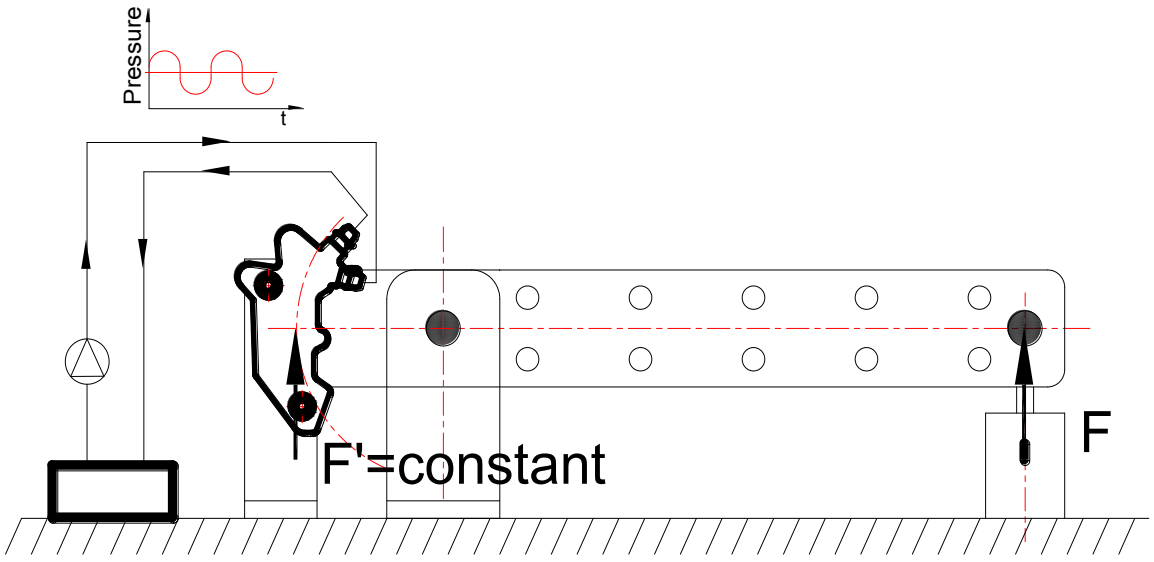

a)

b)

Fig. 5. a) Schematic drawing of the test setup and b) test setup

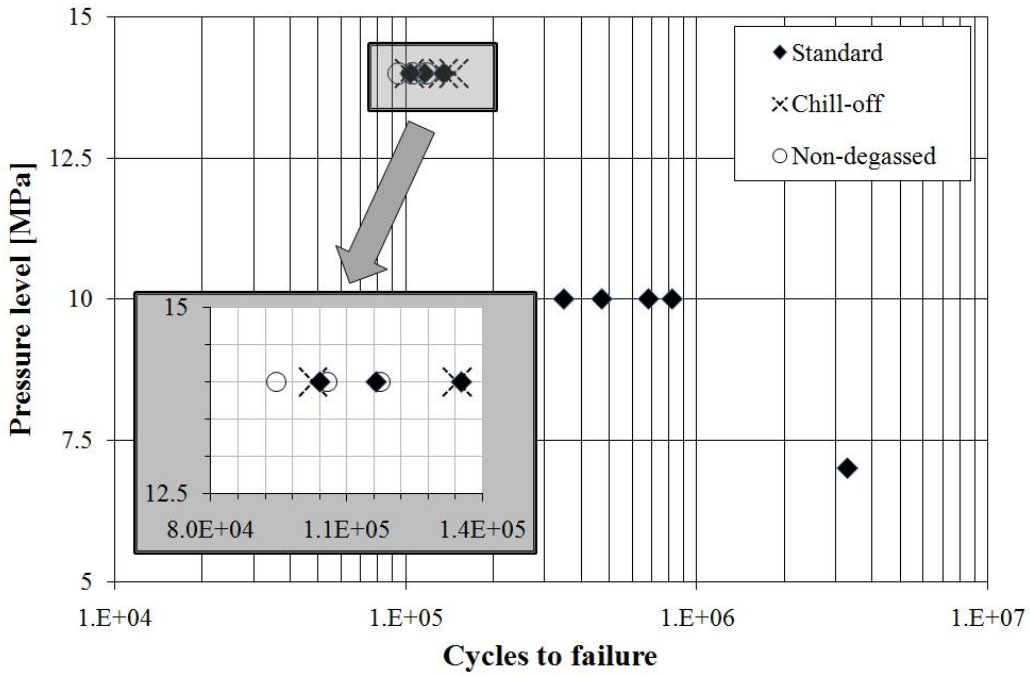

Fig. 6. Results of the fatigue tests on the brake calipers.

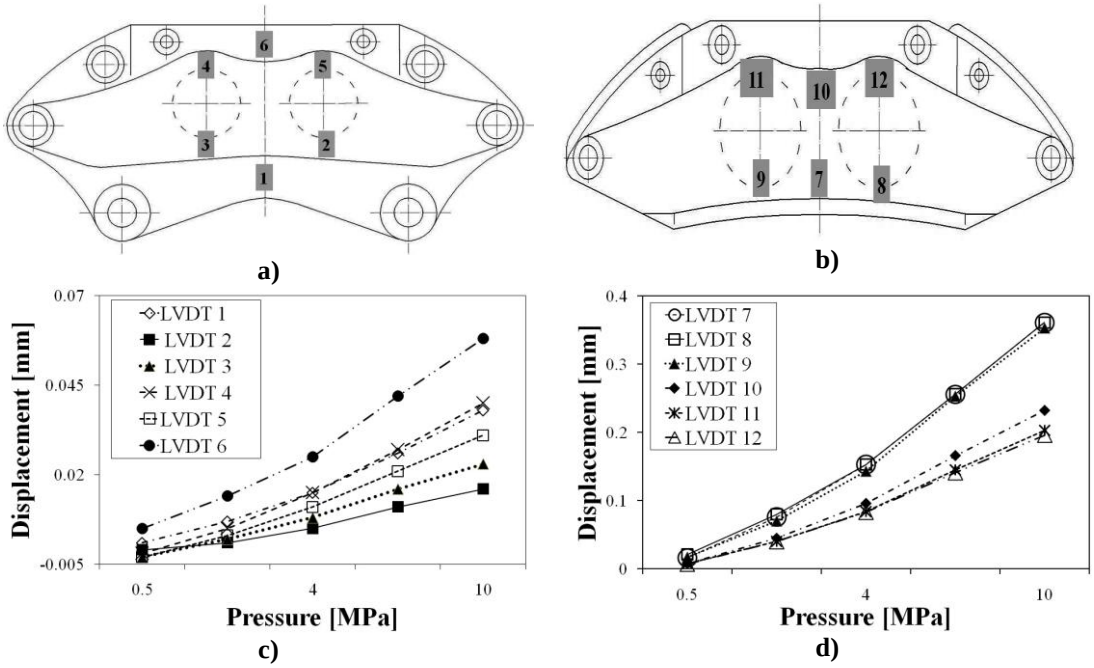

Fig. 7. Maps of the LVDT positions and displacements measured on the internal (a, c) and external (b, d) half-caliper.

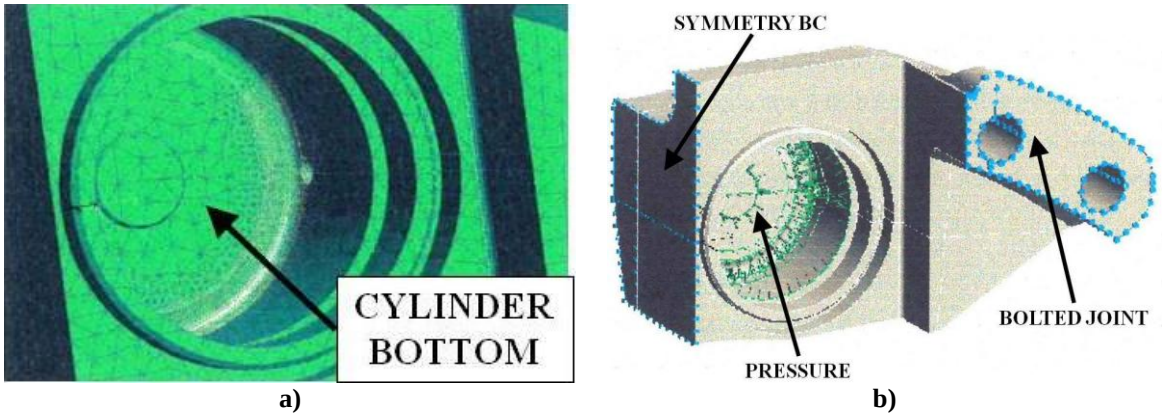

Fig. 8. (a) Mesh refinement at the bottom of the oil cylinder. (b) Loads and boundary conditions.

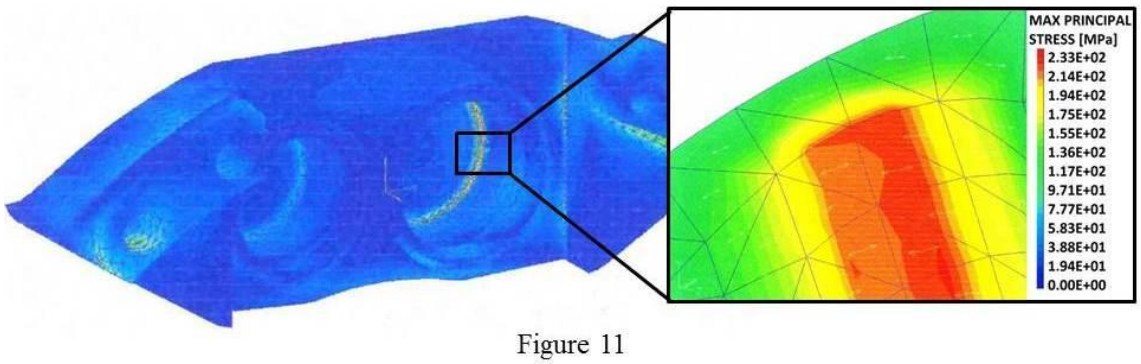

Figure 11

Fig. 9. Map of the maximum principal stress in the whole model and detail of the maximum principal stress at the bottom of the oil cylinder.

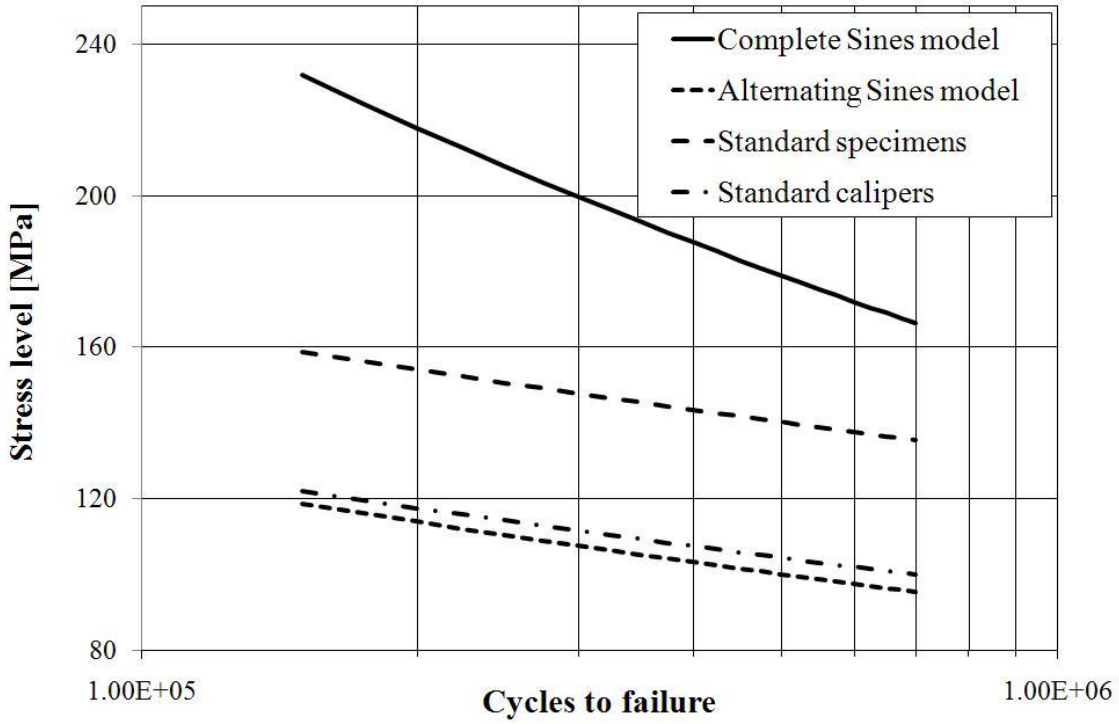

Fig. 10. Stress level vs. cycles to failure diagram: comparison between the predictions with the Sines criterion and the experimental data.

Tables

Table 1
Chemical composition of the castings.

Casting	Si	Mg	Fe	Cu	Mn	Ti	Zn	Na	P	Ni	Pb	Ca	Sr	Sn
Standard	7.007	.552	.154	.003	.006	.112	.001	.0003	.0001	.003	.005	.0009	.003	.002
Non-degassed	7.22	.512	.157	.0036	.006	.109	.001	.0001	.000	.003	.004	.0010	.0035	.002

Table 2
Mechanical characteristics and DAS parameter for each type of casting.

Casting type	Elongation at break [A%]	UTS [MPa]	YS [MPa]	DAS [µm]
Standard	3.5	344	299	26
Chill-off	3.3	328	283	37.5
Non-degassed	3.8	322	246	36

Table 3
Summary of the fatigue tests performed.

Test ID	Calipers #	Caliper type	Oil pressure [MPa]	Braking torque [Nm]	Number of cycles
A	3	Standard	14	/	100,000
B	4	Standard	10	/	350,000
C	4	Standard	10	2,400	350,000
D	3	Non-degassed	14	/	100,000
E	3	Chill-off	14	/	100,000
F	1	Standard	7	/	1,000,000

Table 4.
Results of the fatigue tests on the brake calipers: (a) pulsating pressure tests at 14 MPa, (b) pulsating pressure tests at 10 MPa with and without braking torque.

Brake caliper type	Standard	Chill-off	Non-degassed
Mean n° of cycle	125000	128000	105000
Percentage of standard deviation	12%	3%	14%

a)

Type of test	Pulsating pressure and torque	Pulsating pressure only
Mean n° of cycle	520000	580000
Percentage of standard deviation	26%	31%

b)